Preparation of Calcium Oxalate by Vesicle Modification in the Catanionic Surfactant System CDS/TTABr/H_2O

Renhao Dong, Rui Weng, Yingying Dou, Li Zhang, and Jingcheng Hao*

Key Laboratory of Colloid and Interface Chemistry of Ministry of Education, Shandong University, Jinan 250100, P. R. China

Received: September 9, 2009; Revised Manuscript Received: December 23, 2009

In conventional cationic−anionic (catanionic) surfactant mixtures with excess monovalent salt, two lamellar phase (L_α) regions are usually observed in both the cation-rich and anion-rich solutions, and precipitates form when there is an equal molar ratio of the cationic and anionic surfactants. The phase- and temperature-dependent behavior of the calcium dodecyl sulfate (CDS)−tetradecyltrimethylammonium bromide (TTABr)−water system with excess $CaBr_2$ is reported. A birefringent L_α-phase is observed in the cation-rich solution while the precipitates in both the anion-rich and the cation-rich regions. The introduction of the Ca^{2+} ion is proposed to alter the electrostatic shielding of the surfactant headgroups. Stable vesicles were characterized by TEM and rheology. The formation of the vesicles is driven by electrostatic and hydrophobic interactions between the cationic and anionic surfactants. The results from TEM show that the temperature markedly influences the molecular interactions and changes the structure of molecular bilayers, leading to the instability of the vesicles. The vesicles were used to prepare microcrystals of calcium oxalate monohydrate ($CaC_2O_4 \cdot H_2O$) by adding dimethyl oxalate to L_α solution. X-ray diffraction and scanning electron microscopy indicate that the vesicle phases play an important role in affecting the formation and growth of the CaC_2O_4 crystals. Namely, the microcrystals formed in the reaction are mainly bricklike (dodecahedrons) and starlike (icositetrahedrons). The two morphologies have not been previously observed in COM. Furthermore, they are larger than those prepared without surfactant, which may also explain a role for surfactants in calcium oxalate biomineralization.

Introduction

Catanionic surfactant mixtures have been widely studied because of the appearance of richer phase behavior compared to single-surfactant systems.[1–10] Spontaneous aggregation can occur in catanionic solutions at low concentration, including mixed micelles, vesicles, lamellae, and cubic phases.[1–3] The appearance of these phases is because of ion pair formation after mixing the cationic and anionic surfactants in solution leading to a significant reduction in the equilibrium area per surfactant molecule.[7] Among these aggregates, the formation of vesicles have been extremely attractive because of their potential applications as biological models, drug delivery systems, microreactors, and templates for synthesizing materials.[11,12] The fabrication of vesicles in catanionic surfactant systems have been mostly focused on mixtures with excess monovalent salt formed by their counterions, e.g., aqueous solutions of sodium dodecyl sulfate (SDS) and alkyltrimethylammonium halides.[13–18] These systems display similar phase behavior; i.e., two lamellar (L_α) phase regions are usually observed on both the cation-rich and anion-rich solutions, and precipitates form when there is an equal molar ratio of the cationic and anionic surfactants.

In this paper, the phase behavior of calcium dodecyl sulfate (CDS) and tetradecyltrimethylammonium bromide (TTABr) in water system which has excess divalent salt ($CaBr_2$) is described. The micellization of the anionic surfactant CDS with divalent Ca^{2+} as counterion in water has been rarely reported, because CDS has a very high Krafft point, and its solubility at room temperature is very low in water. When CDS is mixed with medium- and long-chain alcohols in aqueous solution, swollen lamellar and sponge phases are observed.[19–21] Surprisingly, highly dilute iridescent lamellar phases are obtained after addition of SDS to the CDS/octanol/H_2O solution, which indicates that different counterions influence the microstructures and properties of the system.[22] In addition, Hoffmann et al. reported that multilamellar vesicles are first produced in aqueous mixtures of the single-chain zwitterionic surfactant tetradecyldimethylamine oxide (C_{14}DMAO) and the anionic surfactant CDS.[23,24] Conductivity measurements of CDS indicate that Ca^{2+} acts as a cross-link between two dodecyl sulfate ions leading to behavior similar to a double-chain zwitterionic surfactant in water.

Previously, vesicles have been used as soft templates to prepare various materials.[25,26] The advantage of the surfactant vesicle template is that it can simultaneously supply different environments for the growth of materials, including the 'bulk' solution outside the vesicles, the outer surface of the bilayers, the hydrophobic layers and the inner chamber of the vesicle, as shown in Scheme 1.[8] (i) Materials synthesis reactions may occur in the "bulk" vesicular solution. For instance, Horrath et al.[27] prepared CdS or Ag nanoparticles in the inner chamber or the outer layer, respectively, of vesicles generated from dihexadecyl phosphate (DHP). Also, hollow AuPdPtAg spheres of approximately 500 nm in diameter were assembled in tetrabutylammonium bromide (Bu_4PBr) vesicle solutions.[28] Additionally, Bu_4PBr vesicles were used to synthesize Ce-doped Pd nanospheres with hollow chambers.[29] (ii) Additional examples of materials formed inside vesicles include Fe_3O_4 particles formed by entrapping aqueous Fe^{3+}-salt and NaOH in phospholipid unilamellar vesicles.[30] The synthesis of nanometer-size CdS, ZnCdS, and HgCdS particles were performed using L_α-

* To whom correspondence should be addressed. E-mail: jhao@sdu.edu.cn. Fax: +86-531-88366074.

10.1021/jp908736d
Published on Web 01/22/2010

SCHEME 1: A Typical Model of Multilamellar Vesicle Supplying Different Reaction Spaces[8]

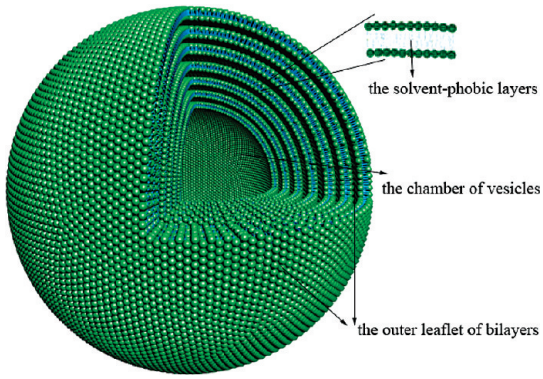

phosphatidylcholine unilamellar vesicles as microreactors.[31] (iii) Reaction occurs on the outer leaflet surface of the bilayers. Hubert et al. prepared SiO_2 spheres by hydrolysis reaction of silicon alkoxide (TMOS) in the dioctadecyldimethylammonium bromide (DODAB) vesicular solution and found that the vesicles were completely covered with silica.[32] Calcium carbonate microcrystals were synthesized by the reaction of $CaCl_2$ and NH_4HCO_3 in an aqueous solution of dipalmitoyldiphosphatidic acid (DPPA) vesicles. The phospholipids were found to be entrapped in the $CaCO_3$ spheres during the crystallization process.[33] (iv) Reaction occurs inside the bilayers. Hubert et al.[34] described the use of DODAB vesicle bilayers as an ordered medium for the free radical polymerization of styrene, and also reviewed the area of vesicle templating.[35] Subsequently, vesicles were formed in aqueous solution of SDS/DTABr (dodecyltrimethylammonium bromide) mixture by Kepczynski et al.[36] and then the hydrolysis of 1,3,5,7-tetramethylcyclotetrasiloxane was carried out inside the bilayers to generate silica materials.

Besides the above vesicle environments, reactions can interact directly with bilayer. In our previous work,[37–39] Zn^{2+} and Ca^{2+} coordination complex vesicles were formed by mixing C_{14}DMAO with zinc 2,2-dihydroperfluorooctanoate [Zn-$(OOCCH_2C_6F_{13})_2$], calcium oleate [Ca$(OA)_2$], or calcium tetradecylamidomethyl sulfate [$(CH_3(CH_2)_{13}NHCOCH_2OSO_3)_2$-Ca]. In these examples, no counterions move freely in the solution, because the metal ions are fixed on the bilayers as a result of coordination. From these coordination vesicles, spherical ZnS nanoparticles, and elongated hexagonal or dumbbell-like $CaC_2O_4 \cdot H_2O$ crystals were prepared on the bilayers by the addition of S^{2-} and $C_2O_4^{2-}$, respectively.

In the present article, we evaluate the phase behavior of calcium dodecyl sulfate (CDS) and tetradecyltrimethylammonium bromide (TTABr) in water with excess divalent salt ($CaBr_2$). A vesicle phase is formed in the cation-rich solution via the cooperation of electrostatic and hydrophobic interactions. The vesicles are used to prepare $CaC_2O_4 \cdot H_2O$ crystals with different morphologies by the reaction of free Ca^{2+} and $C_2O_4^{2-}$, which is distinctly different from our previous synthesis of $CaC_2O_4 \cdot H_2O$ crystals by the combination of bound Ca^{2+} and $C_2O_4^{2-}$.[38] Contrast to the $CaC_2O_4 \cdot H_2O$ crystals obtained in micellar or $CaCl_2$ solutions, vesicles are confirmed to modulate the growth of crystals.

Experimental Section

Chemicals. Sodium dodecyl sulfate ($C_{12}H_{25}SO_4Na$, SDS), tetradecyltrimethylammonium bromide ($C_{14}H_{29}N(CH_3)_3Br$, TTABr), $CaCl_2$, and dimethyl oxalate ($CH_3OOCCOOCH_3$), are of A.R. grade and were used without further purification. Deionized water was used to prepare all sample solutions. Calcium dodecyl sulfate ($Ca(C_{12}H_{25}SO_4)_2$, CDS) was synthesized by combining 100 g of SDS with 34 g of $CaCl_2$ in 1 L of deionized water at 40 °C.[19,40–42] The solution was left standing for about 2 h and then filtered at room temperature. The precipitate was rinsed with deionized water and dried in a vacuum desiccator. The white powder was characterized by ^{1}H NMR and FT-IR (Supporting Information).

Phase Behavior Study and Vesicle Preparation. The phase behavior of the catanionic system was studied by visual inspection, including the assistance of crossed polarizers. Micellar solutions (60 mmol·L^{-1} TTABr) were mixed with increasing amounts of CDS. Mixing was performed at 55.0 °C with stirring and then left thermostated at 52.0 ± 0.1 °C for at least 2 weeks for equilibration. Between C_{CDS} = 14.5 and 25.0 mmol·L^{-1}, a single stable birefringent L_α-phase was observed; this phase is turbid and slightly bluish.[37,38] The phase boundaries were determined by conductivity measurements at 52.0 ± 0.1 °C.

Surface Tension Measurements. Surface tension was measured by a Processor Tensiometer K12 (Switzerland) and the dynamic Wilhelmy plate method using a Pt sheet. The surface tension at various concentrations was measured after equilibration at 52.0 ± 0.1 °C. Each value is the average of three measurements,[43] and the results are within ±0.01 mN·m^{-1}.

Conductivity Measurements. The conductivity measurements were carried out with a DDSJ-308A instrument at 52.0 ± 0.1 °C. The sample solutions of L_1/L_α phase and L_α/precipitate were stirred during the conductivity measurements.

Rheological Measurements. The rheological measurements on the sample solution of the L_α-phase were performed with a HAAKE RS6000 rheometer (Germany) with a coaxial cylinder sensor system (Z41 Ti) at 52.0 ± 0.1 °C. The oscillatory shear frequency was varied from 0.01 to 100 Hz.

Negative-Stained Transmission Electron Microscopy (TEM). Two single stable birefringent L_α-phase solutions of 60 mmol·L^{-1} TTABr and 15 and 17.5 mmol·L^{-1} CDS were prepared at 55.0 °C with stirring and then left thermostated at 52.0 ± 0.1 °C for at least 2 weeks for equilibration. Vesicle structure was determined by negative-stained TEM with phosphotungstic acid as the negative stain dye. About 4 μL of sample solution was placed on a TEM grid (copper, 3.02 mm, 200 mesh, coated with Formvar film) and stained with 2.0 wt % phosphotungstic acid aqueous solution, and the excess solution was blotted with filter paper. After the solution was dried in air, the grids were observed with a JEOL 100CX-II TEM operating at 100 KV.

Freeze−Fracture Transmission Electron Microscopy (FF-TEM). Vesicle structure by FF-TEM images was also performed for a single stable birefringent L_α-phase solution of 60 mmol·L^{-1} TTABr and 17.5 mmol·L^{-1} CDS which was prepared at 55.0 °C with stirring and then left thermostated at 52.0 ± 0.1 °C for at least 2 weeks for equilibration. A small amount of solution to be characterized was placed on a 0.1 mm thick copper disk covered with a second copper disk. The copper sandwich with the sample was frozen by plunging this sandwich into liquid propane which had been cooled by liquid nitrogen. Fracturing and replication were carried out at a temperature of −140 °C. Pt/C was deposited at an angle of 45°. The replicas were examined on a JEOL JEM 100-CXII electron microscope (Japan) at an accelerating voltage of 100 kV.

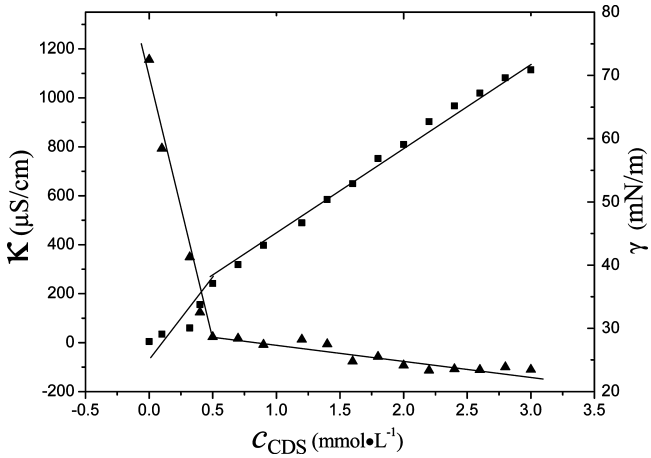

Figure 1. Surface tension (▲) and conductivity (■) as a function of [CDS] at 52.0 ± 0.1 °C. The flex point concentration is (0.50 ± 0.01) × 10^{-3} mol•L^{-1}.

Preparation and Characterization of $CaC_2O_4 \cdot H_2O$ Crystals. A stoichiometric amount of dimethyl oxalate was added to two vesicular solutions of 60 mmol•L^{-1} and 15 mmol•L^{-1} or 17.5 mmol•L^{-1} CDS with stirring, giving a mixture of $n_{Ca^{2+}}$: $n_{C_2O_4^{2-}}$ = 1:1.[38,39] After 10 min stirring, the solution was left standing to equilibrate. To crystallize the CaC_2O_4, the solution was left in a thermostated oven at 52.0 ± 0.1 °C. After 3 days, the precipitates were rinsed with deionized water and ethanol repeatedly and were dried in a vacuum desiccator. TEM was performed on a JEOL JSM6700F field-emission scanning electron microscope (FE-TEM). XRD measurements were carried out on a Japan Rigaku diffractometer using Cu Kα radiation (λ = 1.54178 Å) from a rotating anode X-ray generator operating at 50 kV and 200 mA.

Results and Discussion

Micellization of CDS in Aqueous Solution. Surfactants with multivalent metallic counterions generally have high Krafft points and low solubility. An aqueous solution of SDS (at low concentration) is a clear micellar phase at room temperature. When Na^+ is replaced by Ca^{2+}, the solubility of CDS in water becomes extremely low (K_{sp} = 3.72 × 10^{-10} mol^3•L^{-3}),[19,44] the Krafft point is 50 °C,[40,44] and a 5 mmol•L^{-1} aqueous solution of CDS is clear at 52 °C. CDS is nearly insoluble in alcohol but can be dissolved in DMSO or benzene.

The surface tension and conductivity of CDS solutions as a function concentration at 52.0 ± 0.1 °C are shown in Figure 1. The critical micelle concentration (cmc) can be determined using surface tension and conductivity data according to the flex point of the representative plot. The cmc of CDS is (0.5 ± 0.01) × 10^{-3} mol•L^{-1} at 52.0 ± 0.1 °C, and the surface tension at cmc (γ_{cmc}) is 28.9 mN•m^{-1}. In addition, the surface tension−concentration plot has no minimum, as is usually the case in the presence of surface-active impurities, which is a qualitative indication of the purity of the prepared CDS.

Phase Behavior of the CDS/TTABr/H_2O System. The phase behavior of 60 mmol•L^{-1} TTABr aqueous solution with increasing amounts of CDS up to ~40.0 mmol•L^{-1} at 52.0 ± 0.1 °C is shown in Figure 2. Aqueous TTABr is a low-viscosity L_1-phase solution (cmc = 3.32 × 10^{-3} mol•L^{-1} at 25 °C). With the addition of CDS, a series of phase changes are observed: a clear micellar solution, a micellar/vesicle two-phase region (L_1/L_α-phase), a single vesicle phase solution (L_α-phase), a vesicle/precipitate two-phase region (L_α-phase/precipitate), and a

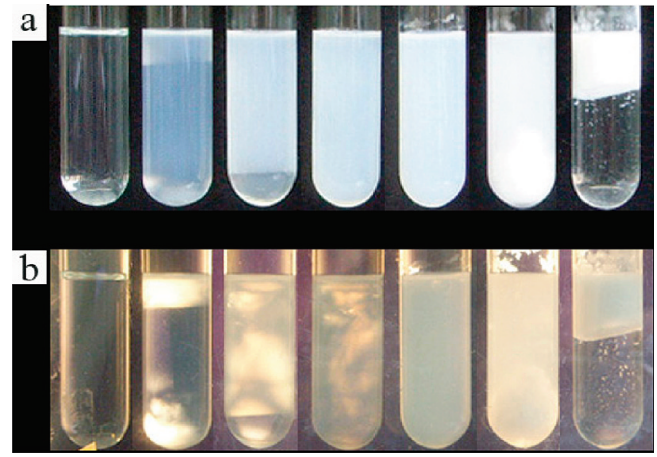

Figure 2. Photographs without (a) and with polarizers (b) of 60 mmol•L^{-1} TTABr aqueous solutions with increasing CDS at 52.0 ± 0.1 °C. The concentrations of CDS and observed phases from left to right are 12.0 mmol•L^{-1} (L_1-phase), 13.0 and 14.0 mmol•L^{-1} (two-phase L_1/L_α), 14.5 and 25.0 mmol•L^{-1} (L_α-phase), 30.0 mmol•L^{-1} (L_α-phase/precipitate), and 40.0 mmol•L^{-1} (L_1-phase/precipitate).

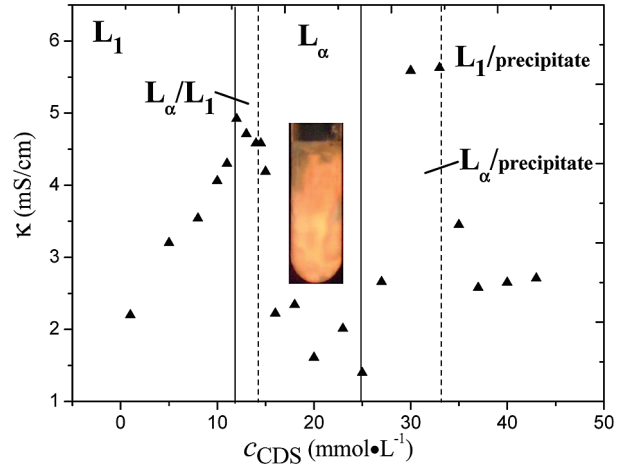

Figure 3. Phase diagram of 60 mmol•L^{-1} TTABr at varied [CDS] in aqueous solution at 52.0 ± 0.1 °C. Conductivity data (▲) are also shown. Inset: photograph of the L_α-phase sample taken with a polarizing filter.

micelle/ precipitate two-phase region (L_1-phase/precipitate). Figure 3 shows the phase diagram of the 60 mmol•L^{-1} TTABr solution with different amounts of CDS, and the different phase boundaries were determined by conductivity measurements. As the concentration of CDS reaches 12.0 mmol•L^{-1}, a single transparent solution is observed, the L_1-phase. With increasing amounts of CDS, a two-phase region presents itself, consisting of a slightly turbid viscous L_α phase on the top and a clear L_1-phase on the bottom (~12.0 to ~14.5 mmol•L^{-1}). A stable and slightly blue and turbid viscous phase was observed from ~14.5 to ~25.0 mmol•L^{-1} CDS. The L_α-phase samples exhibit clear birefringent behavior, confirmed under a polarizer, and is illustrated in the inset of Figure 3. An L_α/precipitate phase occurs from ~25.0 to ~33.0 mmol•L^{-1} CDS, and finally L_1/precipitate phases were observed up to c_{CDS} ≥ 33.0 mmol•L^{-1}.

The phase behavior of CDS/TTABr/H_2O system is significantly different with that of the SDS/TTABr/H_2O system.[9,45] With increasing SDS in a micellar solution of TTABr, the phase changes occur in the order: L_1-phase, micelle/vesicle two-phase region (L_α-phase bottom and a clear L_1-phase on top), single vesicle phase (an L_α-phase with excess TTABr), micelle/precipitate two-phase region (L_1-phase top and precipitate at

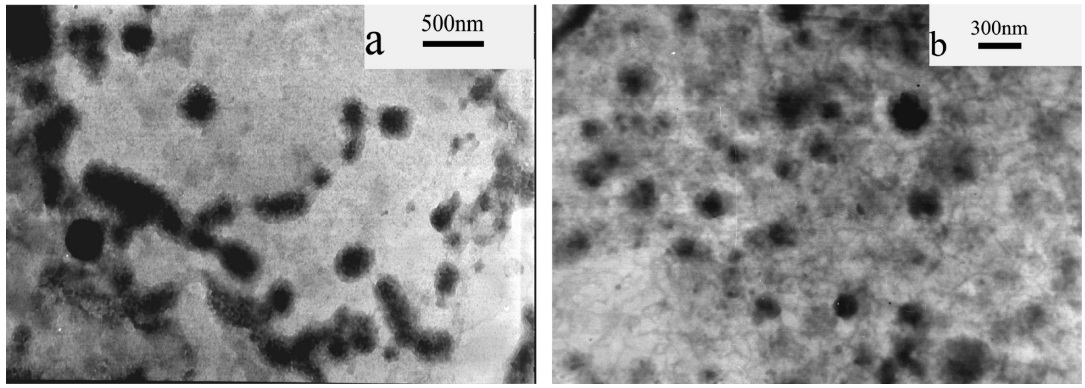

Figure 4. Negative-stained TEM images of L_α-phase solutions at different concentrations: (a) $c_{CDS} = 15.0$ mmol·L^{-1}, and (b) $c_{CDS} = 17.5$ mmol·L^{-1}. A portion of 2.0 wt % phosphotungstic acid is used for coloration at 52.0 ± 0.1 °C.

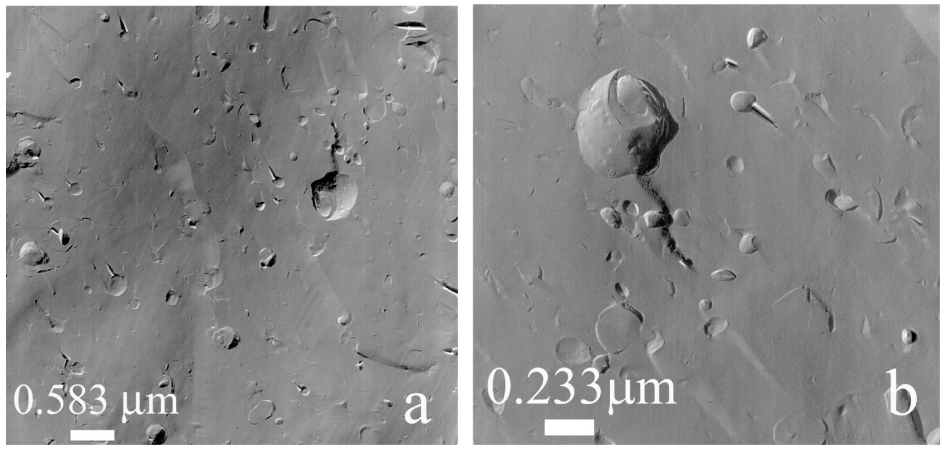

Figure 5. Typical FF-TEM images of 60 mmol·L^{-1} TTABr and 17.5 mmol·L^{-1} CDS L_α-phase solution.

bottom; n_{TTABr}:$n_{SDS} = 1$:1), and finally a single vesicle phase (L_α-phase with excess SDS). Two L_α-phases are observed on the cation-rich and anion-rich sides in the Na^+ system. In the cation-rich region, the vesicles are positively charged, while the vesicles are negatively charged in the anion-rich region. In contrast, only a L_α-phase forms in the cation-rich region of Ca^{2+} system. Compared with SDS, the addition of Ca^{2+} changes the electrostatic shielding, which is thought to cause the difference between the phase behaviors of the two systems.

Formation of Vesicle Phase in Catanionic Surfactant Mixtures. The self-assembled structures of the L_α-phase solution with birefringence were the vesicles, as shown in Figure 4. In this figure, black spherical and ellipsoidal cores with a light ring can be clearly seen, confirming that simply mixing aqueous solution of CDS and TTABr at fixed concentration and temperature leads to the spontaneous formation of stable vesicles. The observed vesicles have a polydispersed size distribution with diameters ranging from about 100 to 300 nm, and it cannot be determined whether the vesicles are unilamellar or multilamellar. On increasing the CDS concentration from 15.0 mmol·L^{-1} (Figure 4a) to 17.5 mmol·L^{-1} (Figure 4b), it is found that the size of vesicles does not markedly change, but the aggregations stack more closely. In Figure 4a, the staining may be a little heavy, and the vesicles look somewhat cohesive.

The typical sample solution of single stable L_α-phase of 60 mmol·L^{-1} TTABr and 17.5 mmol·L^{-1} CDS is birefringent, which can be demonstrated by the strip textures (Supporting Information) of the sample. The strip texture demonstrates the existence of lamellar phase.[46] The lamellar phase contains vesicle which were demonstrated by the FF-TEM micrographs in Figure 5, a and b. It can be seen that most are unilamellar vesicles but a few multilamellar vesicles exist. The vesicular phase should be triggered through the cooperation of electrostatic and hydrophobic interactions, which are completely different from the Ca^{2+}−ligand vesicular system.[38] The size of vesicles is polydispersity with diameter ranging from 20 nm to more than 500 nm which is consistent with those of negative-stained TEM images (Figure 4).

The birefringent L_α-phase sample is highly viscoelastic and exhibits yield stress; i.e., air bubbles may be trapped in these solutions and do not escape for long time; thus, these complex fluids behave like Bingham fluids. A typical rheogram of an L_α-phase with 60 mmol·L^{-1} TTABr and 17.5 mmol·L^{-1} CDS aqueous solution at $T = 52.0 \pm 0.1$ °C is shown in Figure 6. In the oscillatory measurements, the complex viscosity $|\eta^*|$ decreases over the whole frequency range from 0.01 to 5 Hz with a slope of −1. The storage modulus G' and loss modulus G'' are almost frequency independent. The storage modulus G' has a value of approximately 0.95 Pa and is about 1 order of magnitude higher than the loss modulus G'' (about 0.15 Pa). The rheogram of the L_α-phase sample solution has typical characteristics of solutions containing vesicles and behaves in a similar fashion to other vesicular systems.[7,8,12,23,37,38,42,47–52]

Vesicles generally form due to four main driving forces: hydrophobic interactions, electrostatic interactions, hydrogen bonding, or metal−ligand complexation.[53,54] Vesicle formation in the CDS/TTABr/H_2O system is mainly driven by electrostatic and hydrophobic interactions and may be described as follows. Initially, electrostatic attractive interactions cause the mixed ionic surfactants, DS^- and TTA^+, to form an ion-paired monomer, TTA^+−DS^-. Following this, hydrophobic interactions

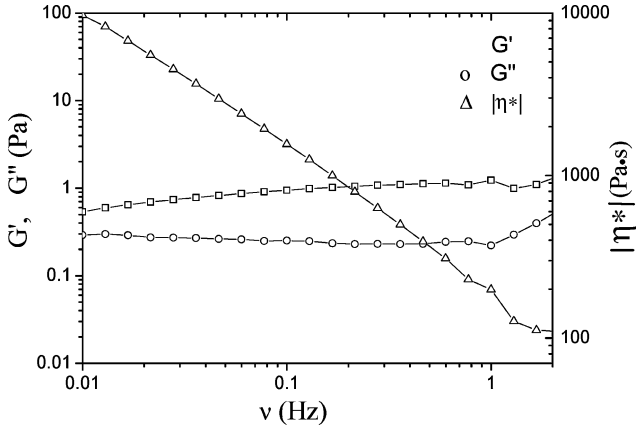

Figure 6. Rheogram of the oscillatory shear for an L_α-phase with 60 mmol·L^{-1} TTABr and 17.5 mmol·L^{-1} CDS aqueous solution at $T = 52.0 \pm 0.1$ °C: $|\eta^*|$ is the complex viscosity (△); G' is the storage modulus (□); G'' is the loss modulus (○); and ν is the scanning frequency.

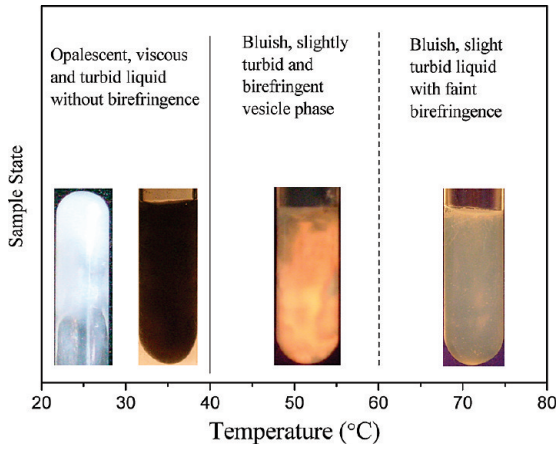

Figure 7. Effect of temperature on the L_α-phase with 60 mmol·L^{-1} TTABr and 17.5 mmol·L^{-1} CDS aqueous solution.

drive the TTA^+-DS^- monomers to form aggregates, but the electrostatic repulsion produced by excess TTA^+ and steric exclusion restrict further aggregation. Therefore, the cooperation of these forces leads to the formation of stable vesicles in bulk solution. However, the introduced Ca^{2+} shields extensively the charge density more than Na^+, which may cause the phase behavior and the macro properties of the CDS/TTABr/H_2O system to be different from those of the SDS/TTABr/H_2O system.

Effect of Temperature on the Stability of Vesicles. The temperature-dependent behavior of the birefringent L_α-phase was examined, as illustrated in Figure 7. The L_α vesicle phase is unstable from room temperature to 70 °C, and the viscosity of the samples changes noticeably. At 25 °C, the sample solution is an opalescent and turbid liquid without birefringence. The liquid is rather viscous and remains in the bottom of an inverted test tube. As the temperature was raised to 40 °C, the sample solution became a slightly blue, turbid, and weakly birefringent liquid. While the viscosity decreased, air bubbles remained trapped inside the solution even with sample agitation. At a solution temperature of about 50 °C, a strong birefringence was observed, and as the temperature increased to above 60 °C, the sample solution was still a bluish and turbid liquid, but with a loss of most of the birefringence. The results suggest that heating changes the structure of the aggregates, leading to the observed bulk properties, and thus the formation of stable vesicles is strongly dependent on the temperature. If the sample solution was cooled from 70 to 50 °C and then thermostated for 24 h, the strong birefringence of the L_α-phase was obtained again. This indicates that the process of vesicle formation by the CDS/TTABr/H_2O mixture is reversible. Our measurements including rheology and TEM were performed at around 50 °C.

Negative-stained TEM observations of a vesicle phase solution in each temperature regime were conducted to observe the changes in the vesicles. As the temperature changed from 25 to 60 °C, a gradual vesicle aggregation process in the 60 mmol·L^{-1} TTABr/17.5 mmol·L^{-1} CDS/H_2O system was observed, whereas disaggregation of the vesicles occurred above 60 °C, illustrated in Figure 8. The most unilamellar vesicles were observed at 52 °C (Figure 8c), which is also demonstrated by the FF-TEM images in Figure 5. At 25 °C, aggregation may occur but vesicles were not observed (Figure 8a). At about 40 °C, only a few nonspherical vesicles were observed and have little cohesiveness (Figure 8b). Above 60 °C, the vesicles disappear completely (Figure 8d).

In comparison, temperature has been generally thought to largely influence the aggregation of amphiphiles in bulk solution, for instance, nonionic poly(oxyethylene) ether surfactants.[55–57] In solutions of these surfactants, high temperature can disrupt hydrogen bonding between water and the poly(oxyethylene) chain, leading to a decrease in the cloud point and causing the phase separation. Below the cloud point, increasing the temperature weakens the hydration of the head groups, which is favorable to the formation of micelles. In addition, the nonionic poly(oxyethylene) ether surfactants in water generally show a rather rich phase behavior with the temperature, mainly because the temperature can lead to changes in the spontaneous mean curvature of the molecular layer, inducing the formation of various aggregates.

The effect of temperature on the vesicle formation by catanionic surfactant mixtures has been rarely reported.[58–60] In the study of the phase behavior of the SDS/dodecyltriethylammonium bromide (DTEABr)/H_2O system,[58] a phase transition from micelle to vesicle was observed upon increasing the temperature. This process is mainly due to the strong interaction between the anionic and cationic surfactants causing the micelles to have similar properties to nonionic surfactants.[59,60] The temperature change leads to a change in the effective surface area per surfactant molecule to drive the phase transitions. Analogously, the temperature changes the phase behavior of the CDS/TTABr/H_2O system. Thus, besides the composition, the formation of the stable vesicles in the CDS/TTABr mixture is mainly induced by the temperature.

Template Preparation of $CaC_2O_4 \cdot H_2O$ Crystals by Vesicles of Catanionic Surfactant Mixtures. Calcium oxalate monohydrate (COM) is the major crystalline material found in human urinary stones. Thus, understanding the modulation of COM crystallization by biomembranes is significant for controlling the disease.[61,62] Vesicles have been used as models of biomembranes and the template synthesis of COM crystals.

The synthesis of $CaC_2O_4 \cdot H_2O$ was performed in the presence of vesicles formed in the CDS/TTABr/H_2O system; the surfactant solution also provides the Ca^{2+} cation. Dimethyl oxalate which was added into vesicular solution may be hydrolyzed to oxalate and methanol. After hydrolysis, calcium oxalate monohydrate precipitates microcrystals ($Ca^{2+} + C_2O_4^{2-} = CaC_2O_4\downarrow$).[38,39] Figure 9 shows SEM images of microcrystals prepared in the vesicle phase of CDS/TTABr/H_2O system (panels a−d), in the aqueous solution of $CaCl_2$ (e), and in the micelle phase of CDS/TTABr/H_2O system (f).

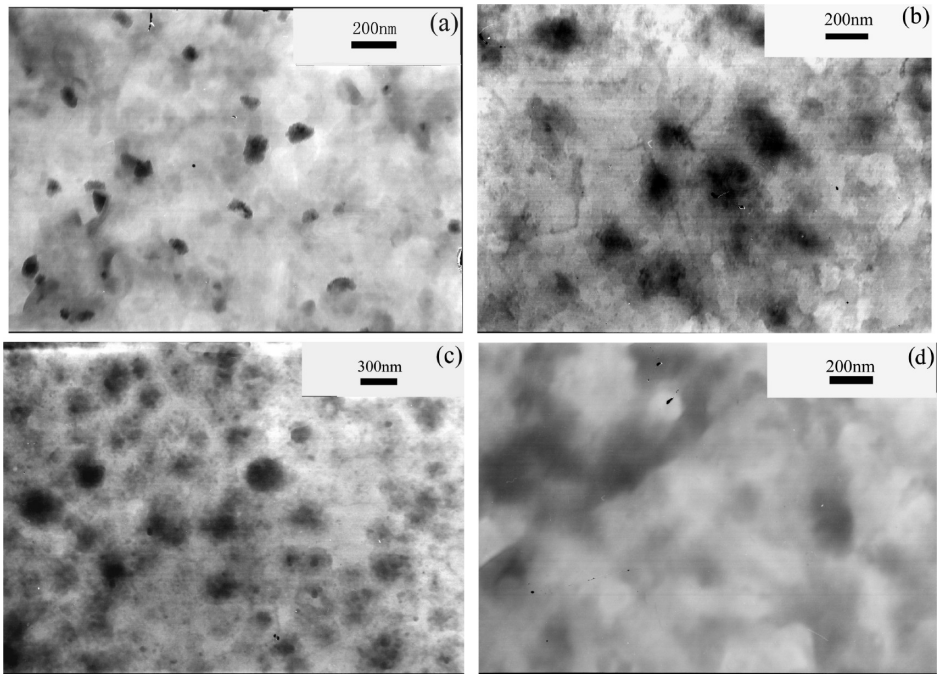

Figure 8. Negative-stained TEM images of the sample solution with 60 mmol·L^{-1} TTABr and 17.5 mmol·L^{-1} CDS aqueous solution; the sample solution was thermostated at 25 °C (a), 40 °C (b), 52 °C (c), and 60 °C (d).

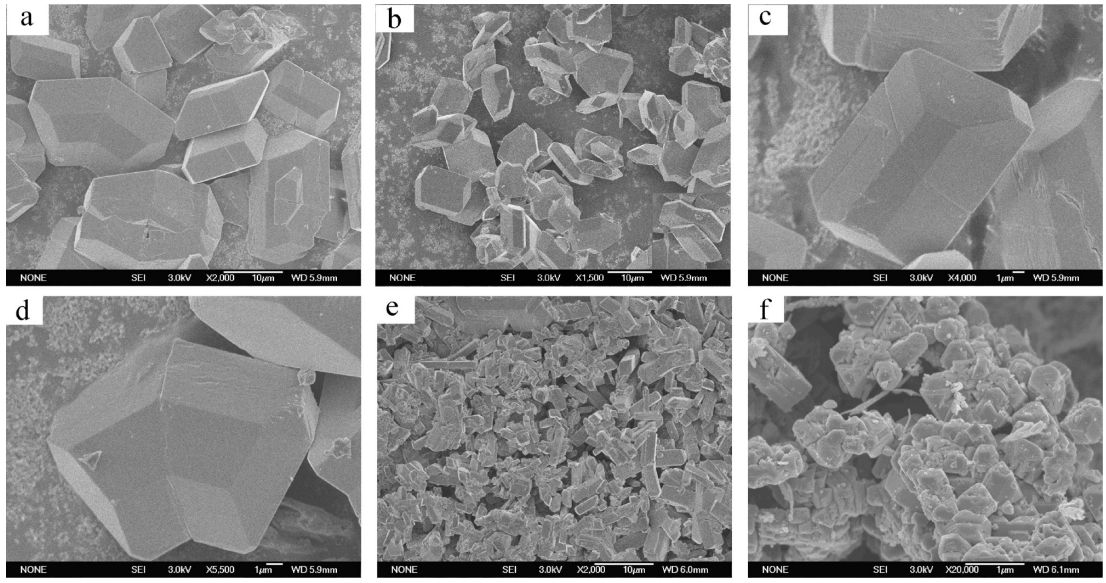

Figure 9. SEM images of CaC_2O_4 crystals grown in different systems: (a) vesicular solution with 60 mmol·L^{-1} TTABr and 15.0 mmol·L^{-1} CDS; (b) vesicular solution with 60 mmol·L^{-1} TTABr and 17.5 mmol·L^{-1} CDS; (c, d) the enlarged images of the two morphologies; (e) aqueous solution of $CaCl_2$ without soft templates; (f) micellar solution with 60 mmol·L^{-1} TTABr and 10.0 mmol·L^{-1} CDS.

When the c_{CDS} = 15.0 and 17.5 mmol·L^{-1}, a large amount of bricklike and starlike crystals were simultaneously obtained by the reaction of Ca^{2+} and oxalate in the vesicular solution (Figure 9, a and b). Enlarged images of the two crystal morphologies are shown in Figure 9 (c and d). It can be seen that the bricklike particles are symmetrical dodecahedra with dimensions of about 11 × 7 × 2 μm ($l \times w \times h$), of which a pair of diagonal positions are planes and five planes are observed from a vertical view. The starlike particles are mirror-symmetrical icositetrahedrons and 12 planes can be seen from a vertical view, of which bilateral angles become planes and one side has a breach to form four planes. To the best of our knowledge, the two morphologies have not been previously observed in CaC_2O_4 crystals.[61–67] The results of XRD show that the corresponding main diffraction peaks are located at 0.595, 0.366, 0.298, and 0.236 nm, suggesting a preferential growth of the ($\bar{1}$01), (020), ($\bar{2}$02), and (130) planes, as seen in Figure 10, a and b, which indicates that calcium oxalate monohydrate (COM) crystals were prepared in the vesicle phase.

To compare with CaC_2O_4 crystals prepared by using vesicles as templates, an amount of CaC_2O_4 crystals was synthesized in the aqueous solution and in the micellar solution. Figure 9e presents the image of the CaC_2O_4 precipitates obtained by mixing 15.0 mmol·L^{-1} $CaCl_2$ solution with dimethyl oxalate. The precipitates prepared by the homogeneous precipitation method showed rectangular rods with a wide range of length from 2 to 8 μm, and were confirmed to be COM by XRD (Figure 10c). In the micellar solution of 60 mmol·L^{-1} TTABr/10.0 mmol·L^{-1} CDS, the CaC_2O_4 precipitates are obtained without clear geometry, as shown in Figure 9f. The XRD

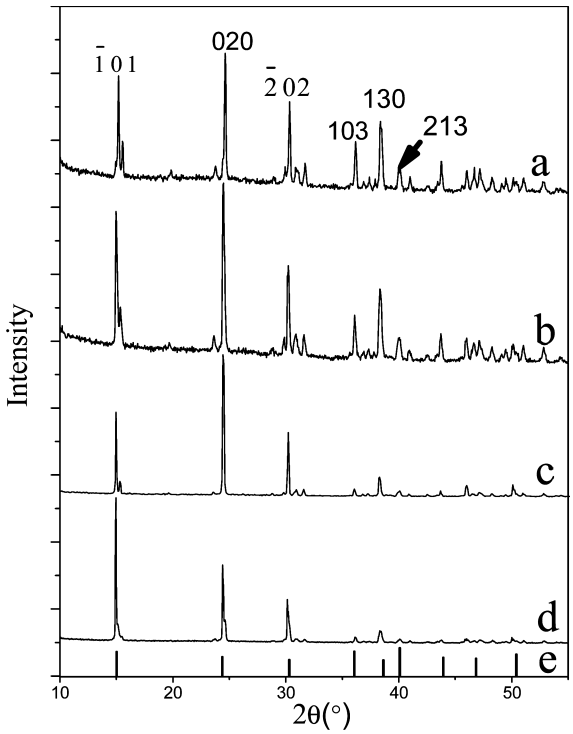

Figure 10. Powder XRD patterns of $CaC_2O_4 \cdot H_2O$ crystals prepared in different systems: (a) vesicular solution of 60 mmol·L^{-1} TTABr and 15.0 mmol·L^{-1} CDS; (b) vesicular solution of 60 mmol·L^{-1} TTABr and 17.5 mmol·L^{-1} CDS; (c) aqueous solution of $CaCl_2$ without soft templates; (d) micellar solution of 60 mmol·L^{-1} TTABr and 10.0 mmol·L^{-1} CDS; and (e) a standard XRD pattern of calcium oxalate monohydrate characterized by the ($\bar{1}$01), (020), ($\bar{2}$02), and (130) peaks.

experiment shows these precipitates are still COM, seen in Figure 10d. The two types of particles are different with those synthesized in the vesicle phase, which indicates that the vesicles play a crucial role in controlling the growth of the CaC_2O_4 crystals.

On increasing the concentration of CDS from 15.0 to 17.5 mmol·L^{-1}, the amount of bricklike particles is found to decrease while the amount of starlike particles increases (Figure 9, a and b), and the diffraction intensity of the (020) face becomes stronger (Figure 10, a and b). Similar phenomena of the effect of vesicular concentration on the crystals were obtained in our previous work on preparing the COM crystals by the hydrolysis of dimethyl oxalate in Ca^{2+}−ligand coordinated vesicle phase solution.[38] Thus, this suggests that the concentration of vesicles may change the morphologies of the obtained precipitates due to the changes of the compactness of the stacking vesicles.

Mechanism of $CaC_2O_4 \cdot H_2O$ Crystal Preparation by Vesicle Template. The preparation of Calcium oxalate in the vesicle of CDS/TTABr/H_2O system is completely different from our previous work in the metal−ligand-coordinated vesicle of the calcium tetradecylamidomethyl sulfate/C_{14}DMAO/water system. In the previous work, Ca^{2+} was bound on the bilayers of the vesicles owing to the coordination interaction, while in the vesicle solution of CDS/TTABr/H_2O system, the Ca^{2+} are free and not the part of the vesicles.

Two kinds of Ca^{2+} ions are separated in the vesicle solution of CDS/TTABr/H_2O system; some are free in the bulk solution, while the others are located inside the chamber of vesicles. After the addition of dimethyl oxalate, reactions can occur simultaneously inside and outside the vesicles. Unlike the random growth of calcium oxalate crystals in pure aqueous solution,

SCHEME 2: Model of Dimethyl Oxalate in the Vesicular Solution of CDS/TTABr/H_2O

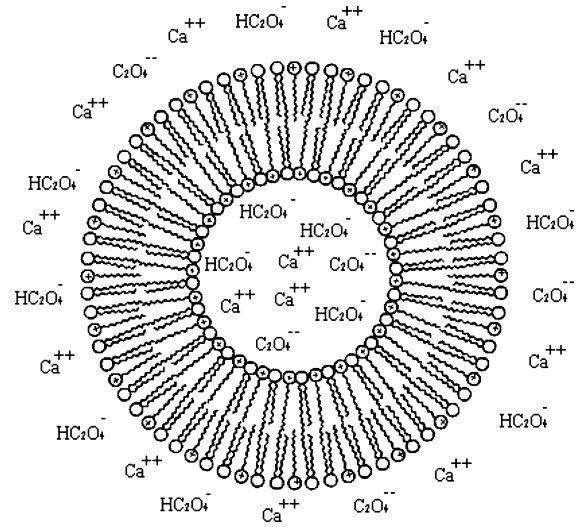

there are two kinds of inhibitions for the COM growth in vesicular solution. One is mentioned in the Introduction: vesicles can supply different spaces for the growth of inorganic particles. Here, two sites are for the nucleation of COM, i.e., the outer bilayers and the chamber of the vesicles. Reactions on the outer bialyers are due to excess TTA^+ inserting into the bilayers causing the positively charged layers to adsorb a large amount of $C_2O_4^{2-}$, which then react with the free Ca^{2+} from the bulk solution, as shown in Scheme 2. In addition, some $C_2O_4^{2-}$ anions enter the chamber of vesicles and combine with the restrained Ca^{2+} cations. Thus, the crystals can grow in the inner of the vesicles and on the outer leaflet of the bilayers. The other inhibition is attributed to preferential adsorption of surfactant at the COM/solution interface.[63] In aqueous solution, COM crystals have a controlled growth habit that ($\bar{1}$01) is the most developed plane with the strongest diffraction peak, as seen in Figure 9d. In the vesicle solution, an electrostatic repulsion occurs between the positively charged surface of the vesicle and the positively charged ($\bar{1}$01) faces of COM crystals[66] and may induce the formation of surfactant layer with ionic headgroups orientated toward liquid solution, leading to the repulsion between the COM crystals. This explanation is in accordance with the patterns in Figure 9a,b; the peak intensity of ($\bar{1}$01) becomes weaker than that of (020), indicating the inhibition of ($\bar{1}$01) faces and the preferential growth of (020) faces. Therefore, space limitation and surfactant adsorption inhibit the crystal growth, finally leading to the formation of the two main morphologies, bricklike and starlike.

It has been shown that the amount of bricklike particles decreases while the amount of starlike particles increases with the increase of the vesicular concentration. It can be extrapolated that bricklike ones may form on the outer leaflet of the bilayers while starlike ones may grow in the inner of the vesicles, because increasing the concentration causes the vesicles to stack more closely, leading to the increase of the number of the inner spaces and the decrease of the number of the outer spaces. In addition, the increase of CDS also changes the effects of surfactant adsorption. However, the mechanism of the formation of the two morphologies needs further investigation.

Conclusion

The catanionic surfactant mixture of CDS and TTABr in water exhibits complex behavior in the cation-rich solution

region; L_1, L_1/L_α, L_α, L_α/precipitate, and L_1/precipitate phases are sequentially observed with the increase of CDS concentration. This phase behavior is different from the conventional SDS/TTABr catanionic surfactant system; i.e., the L_α-phase is observed in the cation-rich region and also in the anion-rich region. In the SDS system precipitates are also obtained when the molar ratio of cationic and anionic surfactant is 1:1. The reason causing the difference is that the introduction of Ca^{2+} changes the electrostatic shielding.

Temperature is found to largely influence the stability of vesicles. On increasing the temperature from room temperature (25 °C) to 70 °C, a phase transition from the formation of vesicles to the disaggregation of vesicles is observed with polarizers and by TEM. The result suggests that vesicles formed by the mixture of CDS and TTABr are strongly dependent on the temperature. It may be due to the strong interactions causing the ionic surfactant to have similar properties to nonionic surfactants, leading to the effective surface area per surfactant molecule being changed by the temperature to drive the phase transitions.

Vesicles formed in the CDS/TTABr/H_2O system are used as template to successfully prepare bricklike (dodecahedron) and starlike (icositetrahedron) calcium oxalate monohydrate (COM) crystals. In contrast, the rodlike COM crystals are prepared in the aqueous solution without the existence of any aggregation and the COM precipitates without clear geometry are synthesized in the micelle phase of the CDS/TTABr/H_2O system. The result indicates that the vesicles can modulate the growth of the inorganic particles. The formation mechanism is also extrapolated to be closely correlated with the special steric configuration of the vesicles and surfactant adsorption.

Acknowledgment. The authors thank the NSFC (Grant No. 20625307) and National Basic Research Program of China (973 Program, 2009CB930103) for financial support, and thank Dr. J. David Van Horn (Visiting Professor, Shandong University) for editorial assistance.

Supporting Information Available: The identification of calcium dodecyl sulfate (CDS) is given, including FT-IR (Figure S1) and ^1H NMR (Figure S2) spectra of CDS, and polarizers of birefringent L_α-phase solution. This material is available free of charge via the Internet at http://pubs.acs.org.

References and Notes

(1) Hudson, S.; Jung, H. T.; Perces, V.; Cho, W. D.; Johansson, G.; Balagurusamy, G.; Balagurusamy, V. S. K. *Science* **1997**, *278*, 449.
(2) Martinez, J. S.; Zhang, G. P.; Holt, P. D.; Jung, H. T.; Carrano, C. J.; Haygoo, M. G.; Butler, A. *Science* **2000**, *287*, 1245.
(3) Pevzner, S.; Regev, O.; Lind, A.; Lindén, M. *J. Am. Chem. Soc.* **2003**, *125*, 652.
(4) Södermann, O.; Herrington, K. L.; Kaler, E. W.; Miller, D. D. *Langmuir* **1997**, *13*, 5531.
(5) Zemb, T.; Dubois, M.; Demé, B.; Gulik-Krzwicki, T. *Science* **1999**, *283*, 816.
(6) Dubois, M.; DeméB.; Gulik-Krzwicki, T.; Dedieu, J. C.; Vautrin, C.; Désert, S.; Perez, E.; Zemb, T. *Nature* **2001**, *411*, 672–675.
(7) Hao, J.; Hoffmann, H.; Horbaschek, K. *J. Phys. Chem. B* **2000**, *104*, 10144.
(8) Song, A.; Dong, S.; Jia, X.; Hao, J.; Liu, W.; Liu, T. *Angew. Chem., Int. Ed.* **2005**, *44*, 4018.
(9) Hao, J.; Hoffmann, H. *Curr. Opin. Colloid Interface Sci.* **2004**, *9*, 279.
(10) Rosoff, E., Ed.; In *Vesicles*; Marcel Dekker: New York, 1996; Surfactant Science Series, Vol. 62.
(11) Pileni, M. P. *Nat. Mater.* **2003**, *2*, 145.
(12) Song, A.; Jia, X.; Hao, J. *Chem.—Eur. J.* **2007**, *13*, 496.
(13) Marques, E. F.; Regev, O.; Khan, A.; Miguel, M. da G.; Lindman, B. *J. Phys. Chem. B* **1998**, *102*, 6746.
(14) Marques, E. F.; Regev, O.; Khan, A.; Miguel, M. da G.; Lindman, B. *J. Phys. Chem. B* **1998**, *103*, 8353.
(15) Bergström, M.; Pedersen, J. S. *Langmuir* **1999**, *15*, 2250.
(16) Bergström, M.; Pedersen, J. S.; Schurtenberger, P.; Egelhaaf, S. U. *J. Phys. Chem. B* **1999**, *103*, 9888.
(17) Bai, G.; Wang, Y.; Wang, J.; Han, B.; Yan, H. *Langmuir* **2001**, *17*, 3522.
(18) Sohrabi, B.; Gharibi, H.; Tajik, B.; Javadian, S.; Hashemianzadeh, M. *J. Phys. Chem. B* **2008**, *112*, 14869.
(19) Hornfeck, U.; Gradzielski, M.; Mortensen, K.; Thunig, C.; Platz, G. *Langmuir* **1998**, *14*, 2958.
(20) Hornfeck, U.; Hammel, R.; Platz, G. *Langmuir* **1999**, *15*, 5232.
(21) Zapf, A.; Hornfeck, U.; Platz, G.; Hoffmann, H. *Langmuir* **2001**, *17*, 6113.
(22) Zapf, A.; Hammel, R.; Platz, G. *Colloids Surf. A: Physicochem. Eng. Aspects* **2001**, *183−185*, 213.
(23) Hoffmann, H.; Gräbner, D.; Hornfeck, U.; Platz, G. *J. Phys. Chem. B* **1999**, *103*, 611.
(24) Zapf, A.; Beck, R.; Platz, G.; Hoffmann, H. *Adv. Colloid Interface Sci.* **2003**, *100−102*, 349.
(25) Vriezema, D. M.; Aragons, M. C.; Elemans, J. A. A. W.; Cornelissen, J. J. L. M.; Rowan, A. E.; Nolte, R. J. M. *Chem. Rev.* **2005**, *105*, 1445.
(26) Zasadzinski, J. A.; Kisak, E.; Evans, C. *Curr. Opin. Colloid Interface Sci.* **2001**, *6*, 85.
(27) Horrath, O.; Fender, J. H. *J. Phys. Chem.* **1992**, *96*, 9591.
(28) Zhang, X.; Li, D. *Angew. Chem., Int. Ed.* **2006**, *45*, 5971.
(29) Li, H.; Liu, J.; Xie, S.; Qiao, M.; Dai, W.; Lu, Y.; Li, H. *Adv. Funct. Mater.* **2008**, *18*, 3235.
(30) Mann, S.; Hannington, J. P.; Williams, R. J. P. *Nature* **1986**, *324*, 565.
(31) Korgel, B. A.; Monbouquette, H. G. *Langmuir* **2000**, *16*, 3588.
(32) Hubert, D. H. W.; Jung, M.; Frederik, P. M.; Bomans, P. H. H.; Meuldijk, J.; German, A. L. *Adv. Mater.* **2000**, *12*, 1286.
(33) Gopal, K.; Lu, Z.; de Villiers, M. M.; Lvov, Y. *J. Phys. Chem. B* **2006**, *110*, 2471.
(34) Jung, M.; Hubert, D. H. M.; Bomans, P. H. H.; Frederik, P. M.; Meuldijk, J.; van Herk, A. M.; Fischer, H.; German, A. L. *Langumir* **1997**, *13*, 6877.
(35) Hubert, D. H. M.; Jung, M.; German, A. L. *Adv. Mater.* **2000**, *12*, 1291.
(36) Kepczynski, M.; Ganachaud, F.; Hémery, P. *Adv. Mater.* **2004**, *16*, 1861.
(37) Wang, J.; Song, A.; Jia, X.; Hao, J.; Liu, W.; Hoffmann, H. *J. Phys. Chem. B* **2005**, *109*, 11126.
(38) Teng, M.; Song, A.; Liu, L.; Hao, J. *J. Phys. Chem. B* **2008**, *112*, 1671.
(39) Song, A.; Hao, J. *Curr. Opin. Colloid Interface Sci.* **2009**, *14*, 94.
(40) Moroi, Y.; Motomura, Y.; Matuura, R. *Bull. Chem. Soc. Jpn.* **1971**, *44*, 2078.
(41) Moroi, Y.; Motomura, K.; Matuura, R. *J. Colloid Interface Sci.* **1974**, *46*, 111.
(42) Moroi, Y.; Oyama, T.; Matuura, R. *J. Colloid Interface Sci.* **1977**, *60*, 103.
(43) Hao, J.; Yuan, Z.; Liu, W.; Hoffmann, H. *J. Phys. Chem. B* **2004**, *108*, 19163.
(44) Lee, R. S.; Robb, I. D. *J. Chem. Soc., Faraday Trans. 1* **1979**, *75*, 2116.
(45) Li, Y.; Hao, J.; Li, G. *J. Dispersion Sci. Technol.* **2006**, *27*, 781.
(46) Regev, O.; Guillemet, F. *Langmuir* **1999**, *15*, 4357.
(47) Li, H.; Hao, J. *J. Phys. Chem. B* **2008**, *112*, 10497.
(48) Hao, J.; Wang, Z.; Liu, W.; Abdel-rahem, R.; Hoffmann, H. *J. Phys. Chem. B* **2004**, *108*, 1168.
(49) Shen, Y.; Hao, J.; Hoffmann, H. *Soft Matter* **2007**, *3*, 1407.
(50) Hao, J.; Song, A.; Wang, J.; Chen, X.; Zhuang, W.; Shi, F.; Zhou, F.; Liu, W. *Chem.—Eur. J.* **2005**, *11*, 3936.
(51) Horbaschek, K.; Hoffmann, H.; Thunig, C. *J. Colloid Interface Sci.* **1998**, *206*, 439.
(52) Yamashita, Y.; Savchuk, K.; Beck, R.; Hoffmann, H. *Curr. Opin. Colloid Interface Sci.* **2004**, *9*, 173.
(53) Svenson, S. *Curr. Opin. Colloid Interface Sci.* **2004**, *9*, 201.
(54) Dong, R.; Wang, L.; Hao, J. *Chin. Sci. Bull.* **2007**, *52*, 2600.
(55) Schick, M. J., Ed.; In *Nonionic Surfactants; Physical Chemistry*; Marcel Dekker: New York, 1987; Surfactant Science Series Vol. 23.
(56) Mitchell, D. J.; Tiddy, G. J. T.; Waring, L.; Bostock, T.; McDonald, M. P. *J. Chem. Soc., Faraday Trans. 1* **1983**, *79*, 975.
(57) Leaver, M. S.; Olsson, U.; Wennerstrom, H.; Strey, R.; Wurz, U. *J. Chem. Soc. Faraday Trans.* **1995**, *91*, 4269.
(58) Yin, H.; Zhou, Z.; Huang, J.; Zheng, R.; Zhang, Y. *Angew. Chem., Int. Ed.* **2003**, *42*, 2188.
(59) Yin, H.; Huang, J.; Lin, Y.; Zhang, Y.; Qiu, S.; Ye, J. *J. Phys. Chem. B* **2005**, *109*, 4104.
(60) Yin, H.; Huang, J.; Gao, Y.; Fu, H. *Langmuir* **2005**, *21*, 2656.

(61) Qiu, S. R.; Wierzbicki, A.; Salter, E. A.; Zepeda, S.; Orme, C. A.; Hoyer, J. R.; Nancollas, G. H.; Cody, A. M.; De Yoreo, J. J. *J. Am. Chem. Soc.* **2005**, *127*, 9036.

(62) (a) Backov, R.; Lee, C. M.; Khan, S. R.; Mingotaud, C.; Fanucci, G. E.; Thalham, D. R. *Langmuir* **2000**, *16*, 6013. (b) Benitez, I. O.; Talham, D. R. *J. Am. Chem. Soc.* **2005**, *127*, 2814.

(63) (a) Skrtic, D.; Filipovic-vincekovic, N.; Füredi-Milhofer, H. *J. Cryst. Growth* **1991**, *114*, 118. (b) Tunik, L.; Addadi, L.; Garti, N.; Füredi-Milhofer, H. *J. Cryst. Growth* **1996**, *167*, 748. (c) Tunik, L.; Füredi-Milhofer, H.; Garti, N. *Langmuir* **1998**, *14*, 3351.

(64) Millan, A. *Cryst. Growth Des.* **2001**, *1*, 245.

(65) Zhang, D.; Qi, L.; Ma, J.; Cheng, H. *Chem. Mater.* **2002**, *14*, 2450.

(66) (a) Ouyang, J.; Duan, L.; Tieke, B. *Langmuir* **2003**, *19*, 8980. (b) Ouyang, J.; Deng, F.; Duan, L. *Colloids Surf. A: Physicochem. Eng. Aspects* **2005**, *257*−*258*, 215. (c) Deng, S.; Ouyang, J. *Cryst. Growth Des.* **2009**, *9*, 82.

(67) Gower, L. B. *Chem. Rev.* **2008**, *108*, 4551.

JP908736D